EUROPEAN ORGANIZATION FOR NUCLEAR RESEARCH

CERN–PH–EP/2005–001
18 January 2005
revised[†)] 22 March 2005

Measurement of the Spin Structure of the Deuteron in the DIS Region

The COMPASS Collaboration

Abstract

We present a new measurement of the longitudinal spin asymmetry A_1^d and the spin-dependent structure function g_1^d of the deuteron in the range $1\ \text{GeV}^2 < Q^2 < 100\ \text{GeV}^2$ and $0.004 < x < 0.7$. The data were obtained by the COMPASS experiment at CERN using a 160 GeV polarised muon beam and a large polarised ^{6}LiD target. The results are in agreement with those from previous experiments and improve considerably the statistical accuracy in the region $0.004 < x < 0.03$.

(Submitted to Physics Letters B)

[†)] author list updated, details added, Fig. 4 modified

The COMPASS Collaboration

E.S. Ageev[24], V.Yu. Alexakhin[8], Yu. Alexandrov[18], G.D. Alexeev[8], A. Amoroso[29], B. Badełek[30], F. Balestra[29], J. Ball[25], G. Baum[1], Y. Bedfer[25], P. Berglund[13], C. Bernet[25], R. Bertini[29], R. Birsa[28], J. Bisplinghoff[3], P. Bordalo[15,a], F. Bradamante[28], A. Bravar[16], A. Bressan[28], E. Burtin[25], M.P. Bussa[29], V.N. Bytchkov[8], L. Cerini[28], A. Chapiro[27], A. Cicuttin[27], M. Colantoni[29,b], A.A. Colavita[27], S. Costa[29], M.L. Crespo[27], N. d'Hose[25], S. Dalla Torre[28], S.S. Dasgupta[6], R. De Masi[20], N. Dedek[19], O.Yu. Denisov[29,c], L. Dhara[7], V. Diaz Kavka[27], A.M. Dinkelbach[20], A.V. Dolgopolov[24], S.V. Donskov[24], V.A. Dorofeev[24], N. Doshita[21], V. Duic[28], W. Dünnweber[19], J. Ehlers[12,16], P.D. Eversheim[3], W. Eyrich[9], M. Fabro[28], M. Faessler[19], V. Falaleev[11], P. Fauland[1], A. Ferrero[29], L. Ferrero[29], M. Finger[22], M. Finger jr.[8], H. Fischer[10], J. Franz[10], J.M. Friedrich[20], V. Frolov[29,c], U. Fuchs[11], R. Garfagnini[29], F. Gautheron[1], O.P. Gavrichtchouk[8], S. Gerassimov[18,20], R. Geyer[19], M. Giorgi[28], B. Gobbo[28], S. Goertz[2,4], A.M. Gorin[24], O.A. Grajek[30], A. Grasso[29], B. Grube[20], A. Grünemaier[10], J. Hannappel[4], D. von Harrach[16], T. Hasegawa[17], S. Hedicke[10], F.H. Heinsius[10], R. Hermann[16], C. Heß[2], F. Hinterberger[3], M. von Hodenberg[10], N. Horikawa[21], S. Horikawa[21], R.B. Ijaduola[27], C. Ilgner[19], A.I. Ioukaev[8], S. Ishimoto[21], O. Ivanov[8], T. Iwata[21], R. Jahn[3], A. Janata[8], R. Joosten[3], N.I. Jouravlev[8], E. Kabuß[16], V. Kalinnikov[28], D. Kang[10], F. Karstens[10], W. Kastaun[10], B. Ketzer[20], G.V. Khaustov[24], Yu.A. Khokhlov[24], N.V. Khomutov[8], Yu. Kisselev[1,2], F. Klein[4], S. Koblitz[16], J.H. Koivuniemi[13], V.N. Kolosov[24], E.V. Komissarov[8], K. Kondo[21], K. Königsmann[10], A.K. Konoplyannikov[24], I. Konorov[18,20], V.F. Konstantinov[24], A.S. Korentchenko[8], A. Korzenev[16,c], A.M. Kotzinian[8,29], N.A. Koutchinski[8], K. Kowalik[30], N.P. Kravchuk[8], G.V. Krivokhizhin[8], Z.V. Kroumchtein[8], R. Kuhn[20], F. Kunne[25], K. Kurek[30], M.E. Ladygin[24], M. Lamanna[11,28], J.M. Le Goff[25], M. Leberig[11,16], J. Lichtenstadt[26], T. Liska[23], I. Ludwig[10], A. Maggiora[29], M. Maggiora[29], A. Magnon[25], G.K. Mallot[11], I.V. Manuilov[24], C. Marchand[25], J. Marroncle[25], A. Martin[28], J. Marzec[31], T. Matsuda[17], A.N. Maximov[8], K.S. Medved[8], W. Meyer[2], A. Mielech[28,30], Yu.V. Mikhailov[24], M.A. Moinester[26], O. Nähle[3], J. Nassalski[30], S. Neliba[23], D.P. Neyret[25], V.I. Nikolaenko[24], A.A. Nozdrin[8], V.F. Obraztsov[24], A.G. Olshevsky[8], M. Ostrick[4], A. Padee[31], P. Pagano[28], S. Panebianco[25], D. Panzieri[29,b], S. Paul[20], H.D. Pereira[10,25], D.V. Peshekhonov[8], V.D. Peshekhonov[8], G. Piragino[29], S. Platchkov[25], K. Platzer[19], J. Pochodzalla[16], V.A. Polyakov[24], A.A. Popov[8], J. Pretz[4], C. Quintans[15], S. Ramos[15,a], P.C. Rebourgeard[25], G. Reicherz[2], J. Reymann[10], K. Rith[9,11], A.M. Rozhdestvensky[8], E. Rondio[30], A.B. Sadovski[8], E. Saller[8], V.D. Samoylenko[24], A. Sandacz[30], M. Sans[19], M.G. Sapozhnikov[8], I.A. Savin[8], P. Schiavon[28], C. Schill[10], T. Schmidt[10], H. Schmitt[10], L. Schmitt[20], O.Yu. Shevchenko[8], A.A. Shishkin[8], H.-W. Siebert[12], L. Sinha[7], A.N. Sissakian[8], A. Skachkova[29], M. Slunecka[8], G.I. Smirnov[8], F. Sozzi[28], V.P. Sugonyaev[24], A. Srnka[5], F. Stinzing[9], M. Stolarski[30], M. Sulc[14], R. Sulej[31], N. Takabayashi[21], V.V. Tchalishev[8], F. Tessarotto[28], A. Teufel[9], D. Thers[25], L.G. Tkatchev[8], T. Toeda[21], V.I. Tretyak[8], S. Trousov[8], M. Varanda[15], M. Virius[23], N.V. Vlassov[8], M. Wagner[9], R. Webb[9], E. Weise[3], Q. Weitzel[20], U. Wiedner[19], M. Wiesmann[20], R. Windmolders[4], S. Wirth[9], W. Wiślicki[30], A.M. Zanetti[28], K. Zaremba[31], J. Zhao[16], R. Ziegler[3], and A. Zvyagin[19]

[1] Universität Bielefeld, Fakultät für Physik, 33501 Bielefeld, Germany[d]
[2] Universität Bochum, Institut für Experimentalphysik, 44780 Bochum, Germany[d]
[3] Universität Bonn, Helmholtz-Institut für Strahlen- und Kernphysik, 53115 Bonn, Germany[d]
[4] Universität Bonn, Physikalisches Institut, 53115 Bonn, Germany[d]
[5] Institute of Scientific Instruments, AS CR, 61264 Brno, Czech Republic[e]
[6] Burdwan University, Burdwan 713104, India[g]
[7] Matrivani Institute of Experimental Research & Education, Calcutta-700 030, India[h]
[8] Joint Institute for Nuclear Research, 141980 Dubna, Moscow region, Russia
[9] Universität Erlangen–Nürnberg, Physikalisches Institut, 91054 Erlangen, Germany[d]
[10] Universität Freiburg, Physikalisches Institut, 79104 Freiburg, Germany[d]
[11] CERN, 1211 Geneva 23, Switzerland
[12] Universität Heidelberg, Physikalisches Institut, 69120 Heidelberg, Germany[d]
[13] Helsinki University of Technology, Low Temperature Laboratory, 02015 HUT, Finland and University of Helsinki, Helsinki Institute of Physics, 00014 Helsinki, Finland
[14] Technical University in Liberec, 46117 Liberec, Czech Republic[e]
[15] LIP, 1000-149 Lisbon, Portugal[f]
[16] Universität Mainz, Institut für Kernphysik, 55099 Mainz, Germany[d]
[17] University of Miyazaki, Miyazaki 889-2192, Japan[i]
[18] Lebedev Physical Institute, 119991 Moscow, Russia
[19] Ludwig-Maximilians-Universität München, Department für Physik, 80799 Munich, Germany[d]
[20] Technische Universität München, Physik Department, 85748 Garching, Germany[d]
[21] Nagoya University, 464 Nagoya, Japan[i]
[22] Charles University, Faculty of Mathematics and Physics, 18000 Prague, Czech Republic[e]
[23] Czech Technical University in Prague, 16636 Prague, Czech Republic[e]
[24] State Research Center of the Russian Federation, Institute for High Energy Physics, 142281 Protvino, Russia
[25] CEA DAPNIA/SPhN Saclay, 91191 Gif-sur-Yvette, France
[26] Tel Aviv University, School of Physics and Astronomy, 69978 Tel Aviv, Israel[j]
[27] ICTP–INFN MLab Laboratory, 34014 Trieste, Italy
[28] INFN Trieste and University of Trieste, Department of Physics, 34127 Trieste, Italy
[29] INFN Turin and University of Turin, Physics Department, 10125 Turin, Italy
[30] Sołtan Institute for Nuclear Studies and Warsaw University, 00-681 Warsaw, Poland[k]
[31] Warsaw University of Technology, Institute of Radioelectronics, 00-665 Warsaw, Poland[l]
[a] Also at IST, Universidade Técnica de Lisboa, Lisbon, Portugal
[b] Also at University of East Piedmont, 15100 Alessandria, Italy
[c] On leave of absence from JINR Dubna
[d] Supported by the German Bundesministerium für Bildung und Forschung
[e] Suppported by Czech Republic MEYS grants ME492 and LA242
[f] Supported by the Portuguese FCT - Fundação para a Ciência e Tecnologia grants POCTI/FNU/49501/2002 and POCTI/FNU/50192/2003
[g] Supported by UGC-DSA II grants, Govt. of India
[h] Supported by the Shailabala Biswas Education Trust
[i] Supported by the Ministry of Education, Culture, Sports, Science and Technology, Japan
[j] Supported by the Israel Science Foundation, founded by the Israel Academy of Sciences and Humanities
[k] Supported by KBN grant nr 621/E-78/SPUB-M/CERN/P-03/DZ 298 2000 and nr 621/E-78/SPB/CERN/P-03/DWM 576/2003-2006
[l] Supported by KBN grant nr 134/E-365/SPUB-M/CERN/P-03/DZ299/2000

Since the surprising result obtained for the spin structure function of the proton by the EMC [1], the determination of the longitudinal spin structure of the proton and the neutron has remained one of the important issues in particle physics [2]. The spin structure functions are used to test the Bjorken sum rule and to determine quark and gluon polarisations from the QCD evolution equations [3]. They are also used as constraints in the derivation of the polarisation of quarks of different flavour from semi-inclusive asymmetries [4, 5].

Here we report on the first results from the COMPASS experiment at CERN on the deuteron spin asymmetry A_1^d and the spin-dependent structure function g_1^d in the deep inelastic scattering (DIS) region, covering the range 1 GeV^2 to 100 GeV^2 in the photon virtuality Q^2 and 0.004 to 0.7 in the Bjorken scaling variable x.

The COMPASS spectrometer is located in the same muon beam line as the former SMC experiment and covers a similar kinematic region for inclusive reactions. However, it uses a higher intensity muon beam of 160 GeV, a longitudinally or transversely polarised target made of ^{6}LiD, and a new two-stage spectrometer. A general description of the experiment has been presented in Ref. [6] and only the most relevant elements for the present analysis will be mentioned below. The data in the longitudinal configuration taken in 2002 and 2003 correspond to luminosities of about 600 pb^{-1} and 900 pb^{-1}, respectively.

The experiment was performed at the M2 muon beam line of the CERN SPS. The muons originate from the decay of π and K mesons produced by the 400 GeV proton beam on a primary beryllium target. The μ^+ intensity is $2 \cdot 10^8$ per spill of 4.8 s with a cycle time of 16.8 s. The beam profile presents a Gaussian core and a large non-Gaussian tail due to halo muons. The beam has a nominal energy of 160 GeV and is focused at the target centre, with a spread of 7 mm (r.m.s.) and a momentum spread of $\sigma_p/p = 0.05$ for the Gaussian core. The momentum of each muon is measured upstream of the experimental area in a beam momentum station consisting of five (four in the year 2002) planes of scintillator strips with a dipole magnet in between. The precision of the momentum determination is typically $\Delta p/p = 0.003$. The incoming muon direction and position are measured by small scintillating fibre hodoscopes and silicon microstrip detectors [7, 8]. The space resolution is about 0.12 mm for the fibres and 0.015 mm for the microstrips, and the direction of the incoming muon is measured with a precision of 30 μrad.

The polarisation P_B of the beam muons was determined by a Monte Carlo program modelling in detail the phase space of the parent hadrons and decay muons, as well as their propagation through the beam transport system [9]. Within a precision of about 0.04 the calculated values are consistent with the polarisation measurements performed by the SMC at 100 and 190 GeV [10]. For the present experiment the model gives a polarisation of the muon varying with its energy from -0.57 at 140 GeV to -0.86 at 180 GeV with a mean value of -0.76.

The target is located inside the solenoid magnet previously used by the SMC experiment [11], which provides a field of 2.5 T along the beam direction. The magnet aperture seen from the upstream end of the target is ± 70 mrad. The target consists of two cells, each 60 cm long and 3 cm in diameter, separated by 10 cm. They are filled with ^{6}LiD which is used as deuteron target material and longitudinally polarised with dynamic nuclear polarisation (DNP) [12]. The two cells are polarised in opposite directions so that data from both spin directions are recorded at the same time. The polarisation is measured by NMR coils with a relative precision of about 5% [13]. The typical polarisation values obtained after a build-up time of about 5 days are $+0.53$ and -0.50. The spin directions in the two target cells are reversed every 8 hours by rotating the magnetic field direction. In this way, fluxes and acceptances cancel out in the calculation of spin asymmetries, provided that the ratio of acceptances remains unchanged after spin reversal. In order to minimise possible acceptance effects related to the orientation of the solenoid field, the

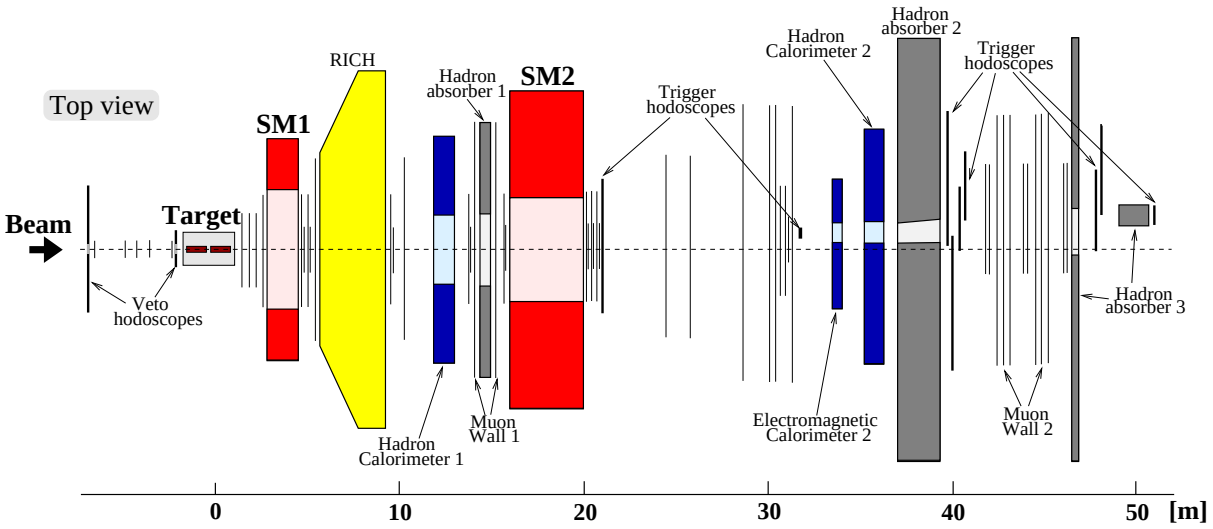

Figure 1: Layout of the COMPASS spectrometer used in 2003. The configuration was identical in 2002 except for Electromagnetic Calorimeter 2 which was not included in the read-out. The thin vertical lines represent the tracking detectors.

sign of the polarisation in each target cell is also reversed several times per year by changing the DNP microwave frequencies.

The COMPASS spectrometer (Fig. 1) is designed to reconstruct the scattered muons and the produced hadrons in wide momentum and angular ranges. It is divided in two stages associated with two dipole magnets, SM1 and SM2. The first one is a large-aperture magnet, with a field integral of 1 Tm along the beam line, which accepts charged particles of momenta larger than 0.4 GeV. The second magnet, SM2, has a field integral of 4.4 Tm and accepts particles of momenta larger than 4 GeV. Different types of tracking detectors are used to cope with the rapid increase of the particle rate from the outside to the central beam region. The beam region downstream of the target is covered by scintillating fibre detectors [7], the region near to the beam by micromesh gaseous chambers [14] and gas electron multiplier chambers [15]. The intermediate region, further away from the beam line, is covered by drift chambers and multiwire proportional chambers. Large-angle tracking is mainly provided by straw detectors [16] and by large drift chambers. The identification of muons is based on the fact that they are observed behind hadron absorbers. Two 'muon wall' detectors are used: the first one, located in front of SM2, consists of two stations of Iarocci-type chambers with an iron layer in between and detects muons outside the aperture of SM2; the second one, installed at the end of the spectrometer, is composed of drift tubes and detects the muons which passed through SM2. Hadrons are detected by two large iron-scintillator sampling calorimeters, installed in front of the absorbers and shielded to avoid electromagnetic contamination.

The data recording system is activated by a combination of signals indicating the presence of a scattered muon at a given angle or in a given energy range. In most DIS events ($Q^2 > 1$ GeV^2), the scattered muon is identified by coincidence signals in the trigger hodoscopes, that define its direction behind SM2. Several veto counters installed upstream of the target are used to avoid triggers due to halo muons. In addition to this inclusive trigger mode, which was commonly used in the previous CERN muon experiments, several semi-inclusive triggers select events fulfilling requirements based on the muon energy loss and on the presence of a hadron signal in the calorimeters [17]. Calorimeter signals due to halo muons are rejected by requiring the presence of at least one cluster with an energy deposit exceeding three times the

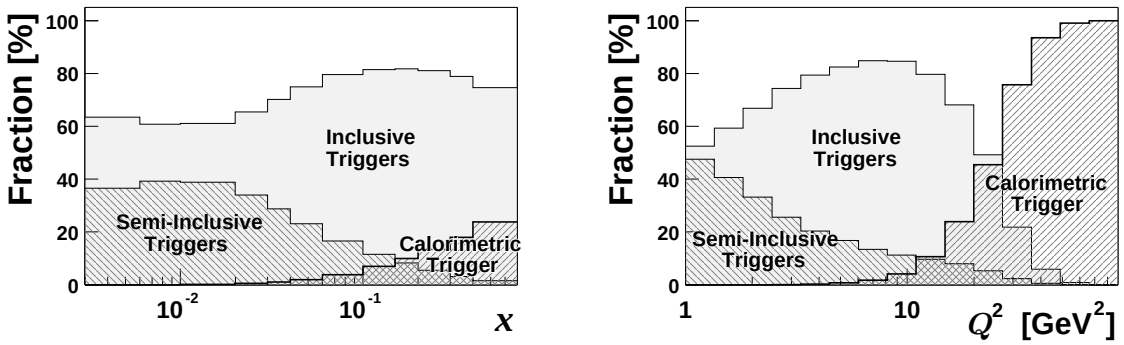

Figure 2: Fraction of inclusive, semi-inclusive, and calorimetric triggers in the final data sample (2002 and 2003) as a function of x (left) and Q^2 (right). Events are counted with the weight they carry in the asymmetry calculation [Eq. (7)].

average value expected for a muon. This condition provides a trigger efficiency of more than 80% for events with total hadronic energy $E_{had} > 30$ GeV. In a part of the 2003 data taking, the acceptance was further extended towards high Q^2 values by the addition of a standalone calorimetric trigger in which no condition is set for the scattered muon but an energy deposit in the hadron calorimeter exceeding 9 times the typical muon response is required. The semi-inclusive and calorimetric triggers thus select a sample of hadronic events which are analysed in parallel with the inclusive sample. The relative contributions of the different trigger types are shown as a function of x and Q^2 in Fig. 2. The fraction of inclusive triggers, where the selection criteria refer only to the scattered muon, varies from 60% to 75% over the range of x (events satisfying simultaneously inclusive and non-inclusive trigger conditions are counted as inclusive). The semi-inclusive triggers account for about 40% of the data at low x and decrease steadily for $x > 0.02$, while the contribution of the standalone calorimetric trigger starts around $x = 0.02$ and reaches 30% in the highest x bin.

Larger variations of the different contributions are observed as a function of Q^2: the inclusive triggers account for 80% of the events at medium Q^2 (3–15 GeV^2), while the standalone calorimetric trigger becomes dominant for $Q^2 > 30$ GeV^2.

In order to eliminate spurious triggers as well as badly or partially reconstructed events, a reconstructed interaction point connected to a beam muon and to a scattered muon is required for all events. In addition, the presence of a hadron track at the interaction point is required for the semi-inclusive and standalone calorimetric triggers. The track reconstruction efficiency was found to be about 95% for scattered muons and for high-energy hadrons ($E > 30$ GeV) that were generated in a Monte Carlo simulation, tracked through the spectrometer, and analysed in the same way as the data. The direction of tracks reconstructed at the interaction point is determined with a precision better than 0.2 mrad and the momentum resolution for scattered muons is about 0.5%.

As the COMPASS trigger setup is predominantly intended for the study of quasi-real photon interactions, DIS events represent only a small fraction of the data sample. The combination of cuts on the photon virtuality ($Q^2 > 1$ GeV^2), the fraction of energy carried away by the virtual photon ($0.1 < y < 0.9$), and the requirement that the interaction take place within one of the target cells results in a reduction factor of about 20. In addition, the incoming muon momentum is required to be in the interval 140 GeV $< p_\mu < 180$ GeV and, in order to equalise fluxes seen by the two target cells, its trajectory is required to cross entirely both target cells. For

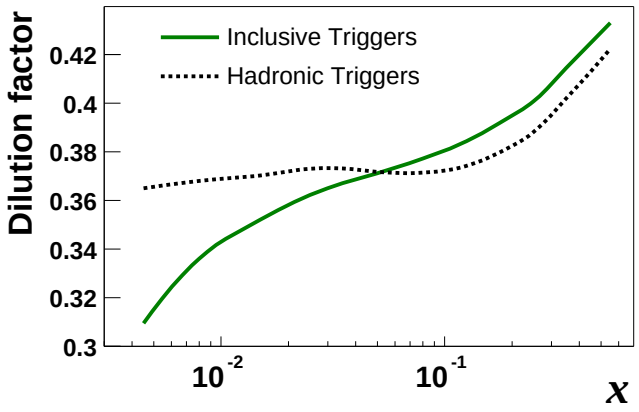

Figure 3: The dilution factor f of the ^{6}LiD polarised target as a function of x for inclusive and hadronic events. The dilution due to radiative effects on the deuteron is included. The values quoted for each x bin are averaged over the kinematic range of the corresponding triggers.

consistency, in events triggered by hodoscope signals, it is also verified that the reconstructed scattered muon hits the hodoscopes that have generated the event trigger. The resulting sample amounts to about $34 \cdot 10^6$ events with a fraction of 71% of the data collected in 2003.

The cross-section asymmetry $A^d = (\sigma^{\uparrow\downarrow} - \sigma^{\uparrow\uparrow})/(\sigma^{\uparrow\downarrow} + \sigma^{\uparrow\uparrow})$, for antiparallel ($\uparrow\downarrow$) and parallel ($\uparrow\uparrow$) spins of the incoming muon and the target deuteron, is related to the virtual-photon deuteron asymmetries A_1^d and A_2^d by

$$A^d = D(A_1^d + \eta A_2^d) \,, \tag{1}$$

where the factors η and D depend on the event kinematics. The virtual-photon depolarisation factor

$$D \simeq \frac{y(2-y)}{y^2 + 2(1+R)(1-y)} \tag{2}$$

depends in addition on the unpolarised structure function $R = \sigma_L/\sigma_T$. The longitudinal virtual-photon deuteron asymmetry is defined as

$$A_1^d = (\sigma_0^T - \sigma_2^T)/(2\sigma^T) \,, \tag{3}$$

where σ_J^T is the virtual-photon–deuteron absorption cross-section for total spin projection J in the photon direction, and $\sigma^T = (1/3)\,(\sigma_0^T + \sigma_1^T + \sigma_2^T)$ is the total transverse photo-absorption cross-section. The transverse asymmetry A_2^d has been accurately measured [18] and was found to be small. Since the kinematic factor $\eta = \frac{2(1-y)}{y(2-y)}\sqrt{Q^2}/E_\mu$ is also small in the COMPASS kinematic range, the second term in Eq. (1) can be neglected, so that

$$A_1^d \simeq A^d/D \,, \tag{4}$$

and the longitudinal spin structure function is given by

$$g_1^d = \frac{F_2^d}{2\,x\,(1+R)} A_1^d \,, \tag{5}$$

where F_2^d is the deuteron spin-independent structure function. The number of events N_i collected from a given target cell in a given time interval is related to the spin-independent cross-section $\overline{\sigma}$ and to the asymmetry A_1^d by

$$N_i = a_i \phi_i n_i \overline{\sigma}(1 + P_B P_T f D A_1^d) \,, \tag{6}$$

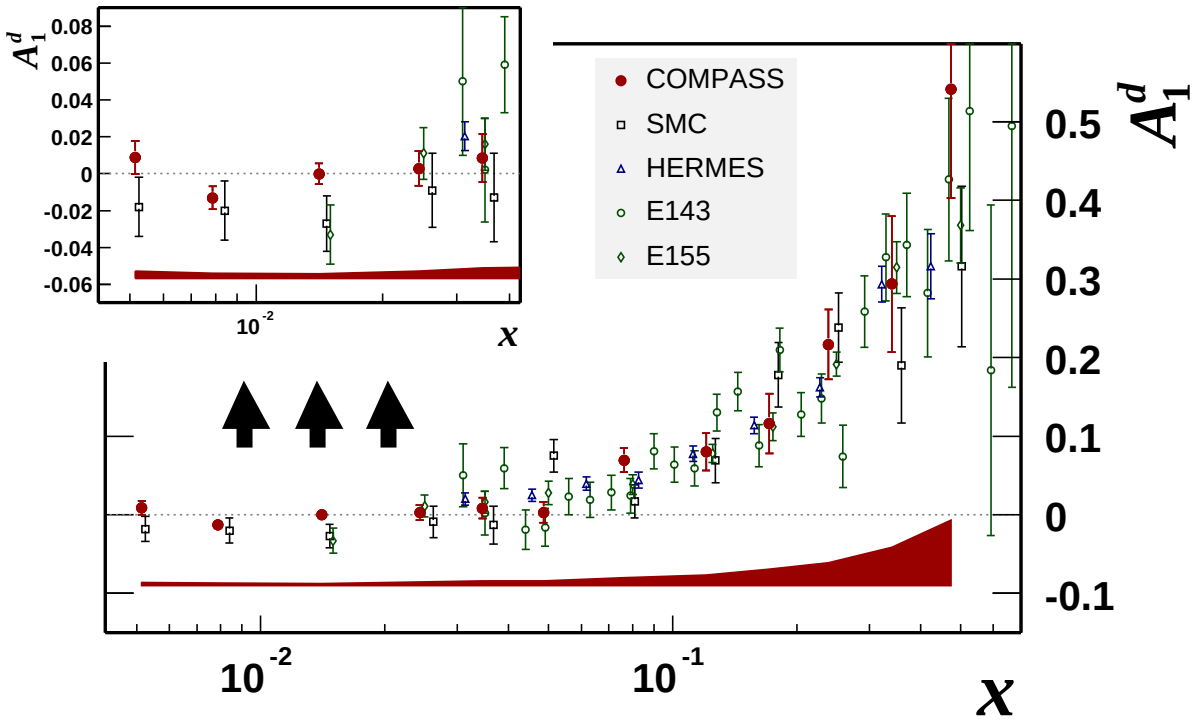

Figure 4: The asymmetry $A_1^d(x)$ as measured in COMPASS and previous results from SMC [25], HERMES [5], SLAC E143 [26] and E155 [27] at $Q^2 > 1$ GeV^2. The SLAC values of g_1/F_1 have been converted to A_1 and the E155 data corresponding to the same x have been averaged over Q^2. Only statistical errors are shown with the data points. The shaded areas show the size of the COMPASS systematic errors.

where P_B and P_T are the beam and target polarisations, ϕ_i the incoming muon flux, a_i the acceptance for the target cell, n_i the corresponding number of target nucleons, and f the target dilution factor. For a ^{6}LiD target the dilution is naively expected to be of the order of 50% because ^{6}Li can be described as an ^{4}He core and a deuteron [19]. The dilution factor f is given by the ratio of the absorption cross-sections on the deuteron to that of all nuclei entering the target cells. It includes a correction for the relative polarisation of deuterons bound in ^{6}Li with respect to free deuterons. It also includes the dilution due to radiative events on the deuteron, which is taken into account by the ratio of the one-photon exchange cross-section to the total cross-section $\rho = \sigma_d^{1\gamma}/\sigma_d^{tot}$ [20]. The values of f are shown in Fig. 3 as a function of x for inclusive and hadronic events. The large difference observed at low x results from the factor ρ which is much smaller in the inclusive case because radiative effects in elastic scattering largely contribute in the denominator. The dilution factors also differ slightly at high x because the inclusive and standalone calorimetric triggers cover different ranges of Q^2 as shown in Fig. 2.

The asymmetry is extracted from data sets taken before and after a reversal of the target spin directions. The four relations of Eq. (6), corresponding to the two cells (u and d) and the two spin orientations (1 and 2), lead to a second-order equation in A_1^d for the ratio $(N_{u,1}N_{d,2})/(N_{d,1}N_{u,2})$. Fluxes and acceptances cancel out in this equation if the ratio of acceptances for the two cells is the same before and after the reversal [21]. In order to minimise the statistical error, all quantities used in the asymmetry calculation are evaluated event by event

Table 1: Values of A_1^d and g_1^d with their statistical and systematical errors as a function of x with the corresponding average values of Q^2 and y.

x range	$\langle x \rangle$	$\langle Q^2 \rangle$ (GeV^2)	$\langle y \rangle$	A_1^d	g_1^d
0.004−0.006	0.0051	1.18	0.76	$0.009 \pm 0.009 \pm 0.004$	$0.190 \pm 0.195 \pm 0.090$
0.006−0.010	0.0079	1.53	0.64	$-0.013 \pm 0.006 \pm 0.003$	$-0.203 \pm 0.096 \pm 0.047$
0.010−0.020	0.0141	2.28	0.54	$0.000 \pm 0.006 \pm 0.003$	$-0.001 \pm 0.056 \pm 0.025$
0.020−0.030	0.0243	3.38	0.46	$0.003 \pm 0.009 \pm 0.004$	$0.018 \pm 0.059 \pm 0.027$
0.030−0.040	0.0345	4.53	0.43	$0.008 \pm 0.013 \pm 0.006$	$0.039 \pm 0.060 \pm 0.028$
0.040−0.060	0.0486	6.08	0.41	$0.003 \pm 0.013 \pm 0.006$	$0.010 \pm 0.044 \pm 0.020$
0.060−0.100	0.0762	8.74	0.38	$0.069 \pm 0.015 \pm 0.010$	$0.149 \pm 0.033 \pm 0.020$
0.100−0.150	0.1205	12.9	0.35	$0.080 \pm 0.024 \pm 0.013$	$0.103 \pm 0.031 \pm 0.017$
0.150−0.200	0.1717	17.5	0.34	$0.116 \pm 0.038 \pm 0.021$	$0.096 \pm 0.031 \pm 0.017$
0.200−0.300	0.2390	23.9	0.33	$0.217 \pm 0.045 \pm 0.029$	$0.110 \pm 0.023 \pm 0.014$
0.300−0.400	0.3401	34.0	0.33	$0.294 \pm 0.086 \pm 0.048$	$0.074 \pm 0.022 \pm 0.012$
0.400−0.700	0.4740	47.5	0.33	$0.542 \pm 0.139 \pm 0.083$	$0.050 \pm 0.013 \pm 0.007$

with the weight factor

$$w = P_B f D. \tag{7}$$

The polarisation of the beam muon, P_B, is obtained from a parametrisation as a function of the beam momentum. The factors f and D are calculated from the kinematic variables with the value of R taken from the NMC [22] or the SLAC parametrisation [23] for x below or above 0.12, respectively. The target polarisation is not included in the event weight [Eq. (7)] because it may vary in time and generate false asymmetries. An average P_T (≈ 0.5) is used for each target cell and each spin orientation.

Inclusive and hadronic events are analysed separately with the corresponding value of the dilution factor. The additive radiative correction to the asymmetry [21] has also been calculated separately [24] using an input parametrisation of A_1^d fitted to the present data. The values obtained for inclusive and hadronic events differ by 0.0003 in the lowest x-intervals and become nearly equal at higher x. These additive corrections are negligible at low x and reach a maximum value of 0.008 at high x.

The asymmetries obtained for hadronic events are statistically compatible with the inclusive ones and their differences do not show any hint of a systematic dependence on x. This observation agrees with the Monte Carlo study of Ref. [25] which also shows that the selection of hadronic events has no sizeable effect on the evaluation of A_1 for interactions on a deuteron target within the kinematic range and the hadron acceptance of the present experiment.

The final values of A_1^d are obtained by merging the inclusive and hadronic sets weighted according to their statistical errors. They are listed in Table 1 with the corresponding statistical and systematical errors and shown in Fig. 4 in comparison with those obtained by the SMC [25], by E143 [26] and E155 [27] at SLAC, and by HERMES [5]. Good agreement is observed over the full range of x. For the four points with $x < 0.03$, our results reduce the statistical errors of previous measurements by a factor of about 2.5.

Figure 5 shows the values of A_1^d as a function of Q^2 for each interval of x. The results of fits to a constant in each interval of x are shown by the solid lines. They yield an average χ^2-probability of about 0.5 and do not indicate any Q^2 dependence. Some dependence of A_1^d on Q^2 is expected from perturbative QCD because the Q^2 evolutions of spin dependent and spin

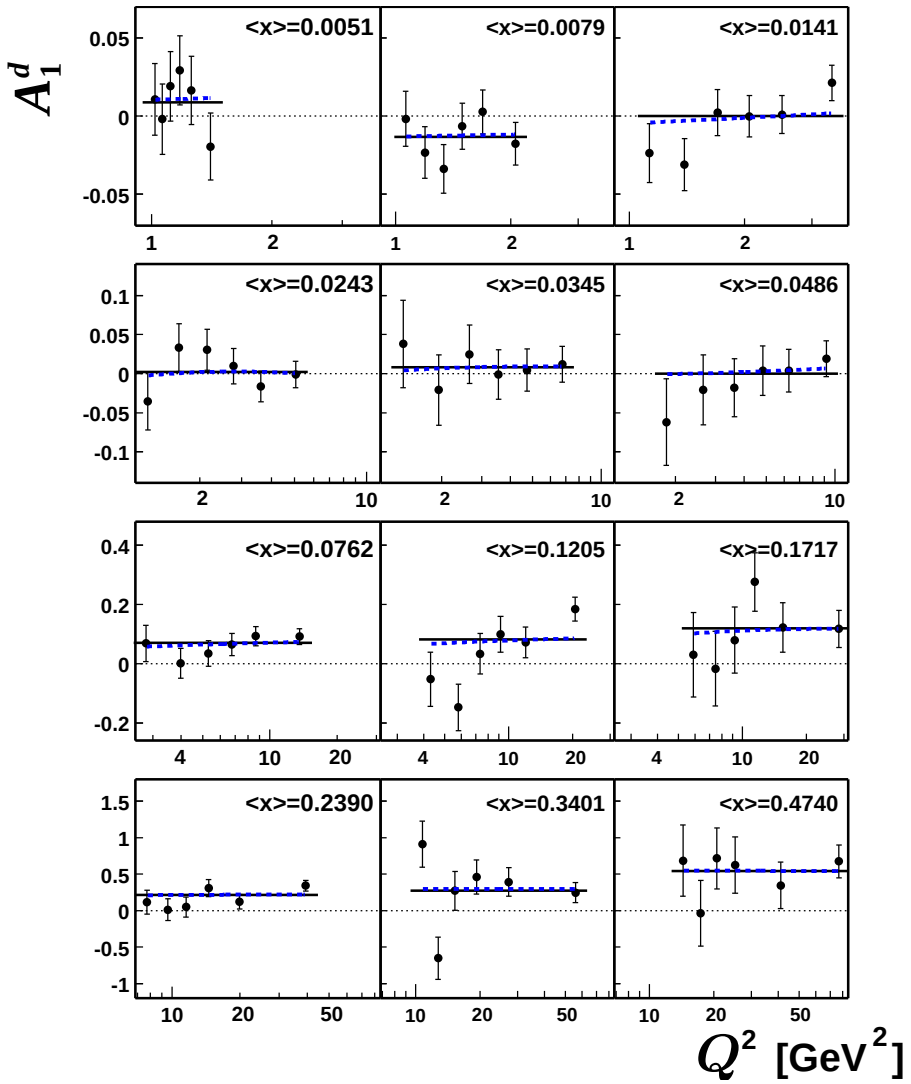

Figure 5: Values of A_1^d as a function of Q^2 in intervals of x. The solid lines are the results of fits to a constant; the dashed lines show the Q^2 dependence predicted by perturbative QCD.

independent structure functions are different. However previous experiments [25] have shown that the two Q^2 evolutions largely cancel out so that the values of A_1^d at fixed x become nearly independent of Q^2. The Q^2 dependence predicted by the SMC fit of Ref. [28] is shown by the dashed lines in Fig. 5 and describes the data equally well.

The systematic error on A_1^d contains an overall scale uncertainty of 6.5% due to the uncertainties on P_B and P_T. The error on the dilution factor f, which takes into account the uncertainty on the target composition and the uncertainty on the corresponding cross-section ratios, is of the order of 6% over the full range of x. The uncertainty on the parametrisation of R affects the depolarisation factor D [Eq. (2)] by 4–5%. The neglect of the A_2 term mainly affects the highest x interval where its contribution is estimated to be ≤ 0.005. The error on the radiative corrections to the asymmetry is estimated by varying the input parametrisation of $A_1^d(x)$ within the statistical error of the present data. The effect of event migration to neighbouring x bins, resulting from the smearing of kinematic variables due to the finite resolution of the spectrometer and to the radiative effects, was evaluated by a Monte Carlo simulation and found to be negligible. Potential false experimental asymmetries were searched for by modifying the selec-

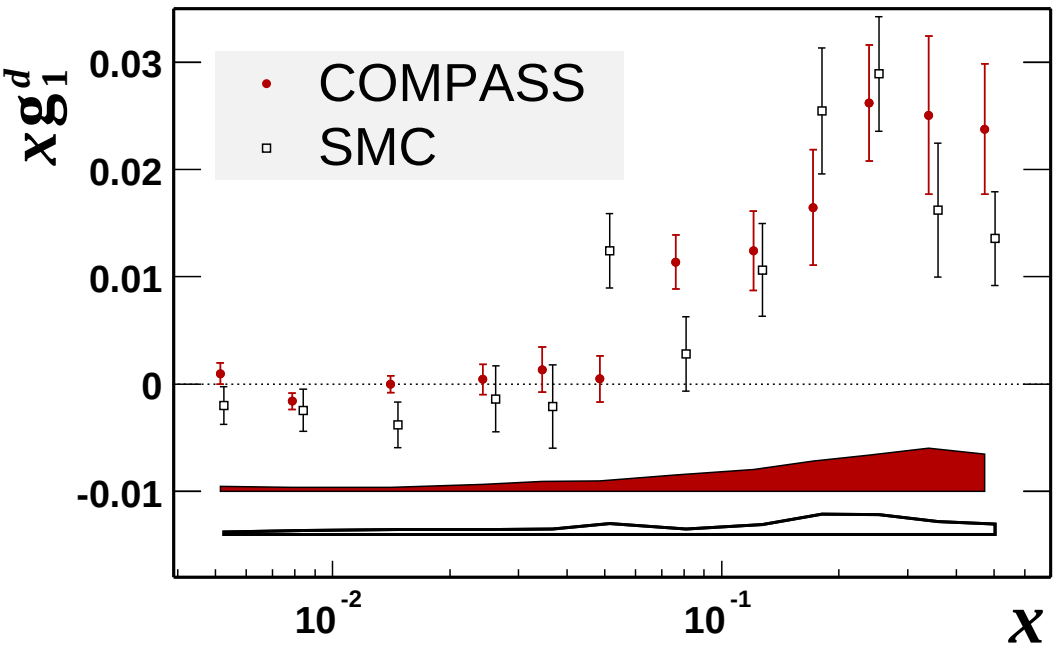

Figure 6: Values of $x\, g_1^d(x)$ *vs.* x. The COMPASS points are given at the $\langle Q^2 \rangle$ of each interval of x. The SMC points [25] were evolved to the Q^2 of the corresponding COMPASS point and are slightly shifted to larger x for clarity. Only statistical errors are shown with the data points. The upper and lower bands show the COMPASS and SMC systematic errors, respectively.

tion of data sets used for the asymmetry calculation. The grouping of data into configurations with opposite target-polarisation was varied from large samples, covering at most two weeks of data taking, into about 100 small samples, taken in time intervals of the order of 16 hours. A statistical test was performed on the distributions of the asymmetries extracted from these small samples. In every interval of x they were found to be normally distributed, with a standard deviation σ compatible with the one derived from the statistical errors (σ_{stat}). Time-dependent effects which would lead to a broadening of these distributions were thus not observed. Since the spread of the observed σ's is about 0.05, we take $1.1\ \sigma_{stat}$ as upper limit for σ and obtain for each x bin a conservative upper bound of the systematic error arising from time-dependent effects

$$\sigma_{syst} < 0.5\ \sigma_{stat}. \tag{8}$$

Asymmetries for configurations where spin effects cancel out were calculated to check the cancellation of fluxes and acceptances. They were found compatible with zero within their statistical errors. The comparison of asymmetries obtained from different parts of the spectrometer did not show any systematic effect. Asymmetries obtained with different settings of the DNP microwave frequency were compared in order to test possible effects related to the orientation of the target field. No sizeable effect was observed.

The values of $g_1^d(x, Q^2)$ quoted in the last column of Table 1 were obtained from Eq. (5), with the F_2^d parametrisation of Ref. [25] and the parametrisation of R already used in the calculation of the depolarisation factor. The systematic errors on g_1^d contain an additional contribution due to the uncertainty on the parametrisation of F_2^d. The error due to the uncertainty on R is reduced by a partial cancellation between the R dependence of the depolarisation factor [Eq. (2)] and the factor $(1 + R)$ in Eq. (5). Our values of g_1^d are shown in Fig. 6 in comparison with

the SMC results [25] which cover the same Q^2 range and were evolved to the same Q^2 values. Their improved accuracy provides a better evaluation of g_1 at low x: integrating the values of $g_1^d(x)$ shown in Fig. 6 over the range $0.004 < x < 0.03$, we obtain $(-0.3 \pm 1.0) \cdot 10^{-3}$ and $(-5.3 \pm 2.3) \cdot 10^{-3}$ for COMPASS and SMC data, respectively. For $x < 0.03$ the COMPASS results are consistent with zero and do not show the tendency of the SMC data of negative g_1^d values.

In combination with the accurate SLAC and HERMES data at larger x, our new results will improve the extrapolation of g_1^d towards $x = 0$. However, taken alone, they do not provide a more accurate evaluation of the first moment Γ_1^d because of the relatively large errors at high x resulting from the late implementation of the calorimetric trigger in the present data. These errors will be reduced for the 2004 data where the calorimetric trigger was used during the full data-taking period.

In conclusion, a new evaluation of the longitudinal spin asymmetry and the spin structure function of the deuteron in the DIS region ($Q^2 > 1$ GeV^2) was performed by the COMPASS experiment at CERN. The data cover nearly the same range of x as the former SMC experiment, $0.004 \leq x \leq 0.7$. The results are in agreement with previous experiments over the full range of x and significantly improve the statistical accuracy in the region $x < 0.03$.

Acknowledgements

We gratefully acknowledge the support of the CERN management and staff and the skill and effort of the technicians of our collaborating institutes. Special thanks are due to V. Anosov, J.M. Demolis and V. Pesaro for their technical support during the installation and the running of this experiment. This work was made possible by the financial support of our funding agencies.

References

[1] EMC, J. Ashman *et al.*, Nucl. Phys. B **328** (1989) 1; Phys. Lett. B **206** (1988) 364.
[2] T.D. Averett, "Nucleon Spin Structure Functions g_1 and g_2 from Polarized Inclusive Scattering", Proc. of the 15th Int. Spin Physics Symposium, AIP Conf. Proc. **675** (2003) 88.
[3] AAC, M. Hirai, S. Kumano and N. Saito, Phys. Rev. D **69** (2004) 054021 and references therein.
[4] SMC, B. Adeva *et al.*, Phys. Lett. B **420** (1998) 180.
[5] HERMES, A. Airapetian *et al.* Phys. Rev. D **75** (2005) 012003.
[6] G.K. Mallot, Nucl. Instrum. Meth. A **518** (2004) 121.
[7] J. Bisplinghoff *et al.*, Nucl. Instrum. Meth. A **490** (2002) 101.
[8] H. Angerer *et al.*, Nucl. Instrum. Meth. A **512** (2003) 229.
[9] N. Doble *et al.*, Nucl. Instrum. Meth. A **328** (1994) 351.
[10] SMC, B. Adeva *et al.*, Nucl. Instrum. Meth. A **443** (2000) 1.
[11] D. Adams *et al.*, Nucl. Instrum. Meth. A **437** (1999) 23.
[12] J. Ball *et al.*, Nucl. Instrum. Meth. A **498** (2003) 101.
[13] K. Kondo *et al.*, Nucl. Instrum. Meth. A **526** (2004) 70.
[14] D. Thers *et al.*, Nucl. Instrum. Meth. A **469** (2002) 133;
C. Bernet *et al.*, Nucl. Instrum. Meth. A **536** (2005) 61.
[15] M.C. Altunbas *et al.*, Nucl. Instrum. Meth. A **490** (2002) 177.
[16] V.N. Bychkov *et al.*, Part. Nucl. Lett. **2** (111) (2002) 64.
[17] J. Hannappel *et al.*, "The COMPASS trigger system for muon scattering", submitted to Nucl. Instrum. Meth. A.
[18] P.L. Anthony *et al.*, Phys. Lett. B **553** (2003) 18.
[19] O.A. Rondon, Phys. Rev. C **60** (1999) 035201 and references therein.

[20] D. Bardin and N. Shumeiko, Sov. J. Nucl. Phys. **29** (1979) 499;
A.A. Akhundov *et al.*, Fortsch. Phys. **44** (1996) 373; Sov. J. Nucl. Phys. **26** (1977) 660;
ibid. **44** (1986) 988.
[21] SMC, D. Adams *et al.*, Phys. Rev. D **56** (1997) 5330.
[22] NMC, M. Arneodo *et al.*, Nucl. Phys. B **483** (1997) 3.
[23] L. Whitlow *et al.*, Phys. Lett. B **250** (1990) 193;
K. Abe *et al.*, Phys. Lett. B **452** (1999) 194.
[24] I.V. Akushevich and N.M. Shumeiko, J. Phys. G **20** (1994) 513.
[25] SMC, B. Adeva *et al.*, Phys. Rev. D **58** (1998) 112001.
[26] E143, K. Abe *et al.*, Phys. Rev. D **58** (1998) 112003.
[27] E155, P.L. Anthony *et al.* Phys. Lett. B **463** (1999) 339.
[28] SMC, B. Adeva *et al.*, Phys. Rev. D **58** (1998) 112002.